Transport in Porous Media (2020) 135:431–456
https://doi.org/10.1007/s11242-020-01482-1

Mathematical Model of Water Alternated Polymer Injection

Bruno J. Vicente[1] · Viatcheslav I. Priimenko[2] · Adolfo P. Pires[2]

Received: 31 March 2019 / Accepted: 15 September 2020 / Published online: 1 October 2020

Abstract
Chemical enhanced oil recovery (EOR) methods include the injection of aqueous polymer solutions slugs driven by water. Polymer solutions increase water viscosity, decreasing the water phase mobility and improving oil recovery through better sweep efficiency. In this paper, we present the water alternated polymer EOR technique, which is based on the injection of successive polymer slugs alternated by water slugs. The mathematical problem is composed by two conservation equations: one of them is related to the water volume and the other one to the polymer mass. We assume that the polymer may be adsorbed by the rock, and the relation between the concentration in the aqueous solution and the solid is governed by a Langmuir type adsorption isotherm. The water viscosity is a function of the polymer concentration in water. The 2×2 system of hyperbolic equations was decoupled by introducing a potential function instead of time as an independent variable. The water alternated polymer injection is represented by a varying boundary condition. The analytical solution presents interactions between waves of different families. It is shown that the polymer slugs always catch up each other along the porous media generating a single slug. As a consequence, the water slugs will disappear. This solution is new and was compared to numerical results with close agreement. It also can be used for the selection of the most suitable enhanced oil recovery technique for a particular oil field.

Keywords Conservation laws · Enhanced oil recovery · Polymer flooding · Flow in porous media

1 Introduction

Polymer flooding is a method of enhanced oil recovery (EOR) appropriate to highly heterogeneous reservoirs, and for cases where oil is displaced by water at unfavorable mobility ratio. Adsorption and the relation between the polymer concentration in water phase and its viscosity are the main phenomena that govern the hydrodynamics of oil displacement by a polymeric solution (Littmann 1988; Sorbie 1991). At equilibrium conditions, the polymer concentration adsorbed on the pore surface can be modeled by

✉ Adolfo P. Pires
adolfo.puime@gmail.com

[1] Universidade Federal do Pará, Salinópolis, Brazil

[2] Universidade Estadual do Norte Fluminense, Macaé, Brazil

an adsorption isotherm, for example, the Langmuir isotherm. To overcome the problem of high cost of the continuous injection of polymer solutions, a finite volume of water containing this chemical product (slug) is injected (Thiele et al. 2010).

Two-phase flow of a polymer solution in porous media (Hatzignatiou et al. 2013, 2015; Zhao et al. 2019) is governed by a 2×2 hyperbolic system of conservation laws (Fayers and Perrine 1958) obtained from the mass balance of the water phase and polymer mass. From this hyperbolic system, Pope et al. (1978) described this chemical flooding process considering the adsorption phenomena and cation exchange. Lake and Helfferich (1978) included the effect of dispersion in the mathematical problem. Pope (1980) applied the fractional flow theory to develop solutions to some of the most common EOR displacement problems; however, the case of slug injection was analyzed only for miscible displacement (gas flooding) and no adsorption. In general, mathematical modeling of oil displacement by polymer solutions injection considers immiscible system. Johansen and Winther (1988) solved the global Riemann problem for a non-strictly hyperbolic system of conservation laws modeling polymer flooding. The problem of multicomponent, multiphase displacement in porous media was analyzed by Helfferich (1981). Johansen and Winther (1989) obtained the exact solution of the Riemann problem modeling multicomponent polymer flooding.

Hyperbolic systems subject to discontinuous initial or boundary conditions lead to interactions of waves of different families (Rhee et al. 1989b; Bedrikovetsky 1993; Smoller 1994). The analytical solutions for this class of problems have been studied in various fields of science and engineering, like shallow water (Sekhar and Sharma 2008), chromatography (Shen 2010), traffic flow (Sun 2009) and gas dynamics (Sekhar and Sharma 2010; Zhang et al. 2008). Mathematically, polymer slug injection is represented by a piecewise boundary condition in which the concentration changes with time (Borazjani et al. 2016a; Torrealba and Hoteit 2019). Bedrikovetsky (1982) described the solution to the problem of the displacement of oil by a polymer slug for different adsorption isotherms. However, the case of water alternated polymer injection was only analyzed for the case of adsorption governed by Henry's law. In this case, all polymer slugs travel with the same velocity in porous media and their speed does not depend on the concentration, leading to a simple solution. The solution for the problem of oil displacement by water alternated polymer slug injection is new and has not been investigated.

Application of a potential function related to the conservation of the aqueous phase as an independent variable instead of time allows the decoupling of the 2×2 hyperbolic system that models polymer flooding in two independent equations (Pires et al. 2004, 2005). One equation depends only on thermodynamic equilibrium conditions (auxiliary equation) and the other depends on the solution of the auxiliary equation and transport properties (lifting equation). This technique was used by Pires and Bedrikovetsky (2005) to develop the analytical solution of the 1-D n-component miscible displacement problem and by Khorsandi et al. (2017) to model low-salinity polymer flooding. For the above-mentioned papers, the splitting of the system of equations simplifies the solution because the equations are solved separately. Using the same technique, Vicente et al. (2014) solved the problem of variable concentration polymer slug considering that adsorption was governed by Langmuir's isotherm. Borazjani et al. (2016b) applied this approach to model the injection of a polymer slug taking into account linear adsorption and change in water salinity. Borazjani et al. (2017) also used this methodology to investigate fines migration in two-phase flow. In the present paper, we apply the decoupling technique to solve the problem of water alternated polymer slugs injection into oil reservoirs. We considered the polymer

adsorption phenomena modeled by a non-linear isotherm. It is important to note that the solution developed here can be used in other methods of enhanced oil recovery, like surfactant flooding.

2 Mathematical Model

The following hypothesis was adopted:

- Newtonian fluids and one-dimensional two-phase flow;
- Homogeneous porous media;
- Incompressible and isothermal system;
- Diffusion, capillary and gravity effects are neglected;
- Liquid and solid phases are in local equilibrium;
- No mass transfer between oil and water phases;
- Polymer concentration does not change the water density.

The velocities of the phases follow Darcy's law (Darcy 1856; Zarand and Pillai 2017):

$$u_w = -\frac{kk_{rw}}{\mu_w}\frac{\partial p}{\partial x'}, \quad u_o = -\frac{kk_{ro}}{\mu_o}\frac{\partial p}{\partial x'} \tag{1}$$

where k is the absolute permeability, p is the pressure, k_{rl} and μ_l are the relative permeability and viscosity, $l = w, o$, and subscripts w and o denote water and oil phases.

The conservation of the water phase is given by

$$\phi\frac{\partial s}{\partial t'} + \frac{\partial u_w}{\partial x'} = 0 \tag{2}$$

and conservation of the polymer mass by

$$\phi\frac{\partial (cs + a(c))}{\partial t'} + \frac{\partial c u_w}{\partial x'} = 0 \tag{3}$$

where ϕ is the rock porosity, s is the water saturation, c is the polymer concentration in the water phase, and $a(c)$ is the polymer concentration on the rock surface (adsorbed).

The water fractional flow is defined as (Bedrikovetsky 1993)

$$f(s,c) = \frac{u_w}{u_w + u_o} = \frac{u_w}{u} \tag{4}$$

where u is the total velocity.

Substituting Eqs. (1) in (4), we obtain an expression for the fractional flow of water, a function of the phases relative permeability and viscosity:

$$f(s,c) = \left(1 + \frac{k_{ro}(s)\mu_w(c)}{k_{rw}(s,c)\mu_o}\right)^{-1} \tag{5}$$

The viscosity of water is an increasing function of polymer concentration, and the concentration of polymer on the rock surface may be determined by Langmuir's adsorption isotherm:

$$a(c) = \frac{\alpha c}{1 + \beta c} \tag{6}$$

where α and β are positive constants of the model determined experimentally.

Substituting Eq. (4) in Eqs. (2)–(3) we obtain the hyperbolic system of conservation laws that models two-phase flow of oil and polymeric solutions in porous media

$$\begin{aligned} &\frac{\partial s}{\partial t'} + \frac{u}{\phi}\frac{\partial f(s,c)}{\partial x'} = 0 \\ &\frac{\partial (cs + a(c))}{\partial t'} + \frac{u}{\phi}\frac{\partial cf(s,c)}{\partial x'} = 0 \end{aligned} \tag{7}$$

Defining the following dimensionless variables:

$$x = \frac{x'}{L} \quad \text{and} \quad t = \frac{1}{\phi L}\int_0^{t'} u(\tau)d\tau \tag{8}$$

where L is the characteristic length of the porous media, and replacing (8) in system (7) we obtain

$$\begin{aligned} &\frac{\partial s}{\partial t} + \frac{\partial f(s,c)}{\partial x} = 0 \\ &\frac{\partial (cs + a(c))}{\partial t} + \frac{\partial cf(s,c)}{\partial x} = 0 \end{aligned} \tag{9}$$

The analytical solution presented in this paper describes the hydrodynamics of oil displacement by water alternated polymer injection. The initial and boundary conditions representing the injection of N polymer slugs in a reservoir initially at uniform water saturation and no dissolved nor adsorbed polymer are given by:

$$t = 0: \begin{cases} s = s^I \rightarrow f(s,c) = 0 \\ c = 0 \end{cases} \quad \text{and} \quad x = 0: \begin{cases} s = s^J \rightarrow f(s,c) = 1 \\ c(t) = \begin{cases} c_n^J, & t_{2n-2}^J \le t \le t_{2n-1}^J \\ 0, & t_{2n-1}^J < t < t_{2n}^J \end{cases}, \quad n = 1, 2, \ldots, N \end{cases} \tag{10}$$

where t_0^J is equal zero, s^I is the initial water saturation, s^J is the water saturation at the inlet face and c_n^J stands for the injected polymer concentration in the *n-th* slug.

2.1 Riemann Problem

The solution of system (9) subject to initial and boundary conditions (10) when $t < t_1^J$ is a Riemann problem, and its solution is composed by rarefaction and shock waves and constant states (Johansen and Winther 1988; Bedrikovetsky 1993).

The rarefaction waves take place in regions where the solution is continuous. There are two different kinds: *s*-waves and *c*-waves. Along an *s*-wave the concentration is constant; on the other hand, along a *c*-wave both saturation and concentration change according to the following ordinary differential equation:

$$\frac{\mathrm{d}c}{\mathrm{d}s} = \left(\frac{f(s,c)}{s + a'(c)} - f_s'(s,c)\right) f_c'(s,c)^{-1} \tag{11}$$

where

$$f_s'(s,c)=\frac{\partial f(s,c)}{\partial s},\quad f_c'(s,c)=\frac{\partial f(s,c)}{\partial c}\quad\text{and}\quad a'(c)=\frac{\mathrm{d}a(c)}{\mathrm{d}c}.$$

System (9) admits two shock waves according to the Rankine–Hugoniot conditions. If the concentration is constant through the shock, it is called an s-shock, and its velocity is given by

$$\frac{\mathrm{d}x}{\mathrm{d}t}=\frac{\left[f(s,c)\right]}{[s]}=\frac{f\left(s^+,c^+\right)-f(s^-,c^-)}{s^+-s^-} \tag{12}$$

where $\left(s^+,c^+\right)$ and (s^-,c^-) are the right and left states, respectively. Across a c-shock, both saturation and concentration change. The velocity of a c-shock is given by

$$\frac{\mathrm{d}x}{\mathrm{d}t}=\frac{\left[cf(s,c)\right]}{[cs+a(c)]}=\frac{f\left(s^+,c^+\right)}{s^++V^{-1}}=\frac{f(s^-,c^-)}{s^-+V^{-1}} \tag{13}$$

where

$$\frac{1}{V}=\frac{[a(c)]}{[c]}=\frac{a\left(c^+\right)-a(c^-)}{c^+-c^-} \tag{14}$$

The complete solution of the Riemann problem is described by a wave sequence linking the boundary condition (left state) to initial condition (right state). An s-wave with zero polymer concentration will be denoted by $\xrightarrow{R_s^0}$ and with constant concentration c_n^J by $\xrightarrow{R_s^J}$. An s-shock and a c-shock are represented by $\xrightarrow{D_s}$ and $\xrightarrow{D_c}$, respectively. Using the aforementioned notation the self-similar solution (Fig. 1) is given by $J\xrightarrow{R_s^J}s_1^-\xrightarrow{D_c}s_1^+\xrightarrow{D_s}I$ if $s_1^+<s_F$ and by $J\xrightarrow{R_s^J}s_1^-\xrightarrow{D_c}s_1^+\xrightarrow{R_s^0}s_f\xrightarrow{D_s}I$ if $s_1^+>s_F$, where J and I are the injection and initial conditions, respectively.

2.2 Coordinate Transformation

Defining a new independent variable φ as

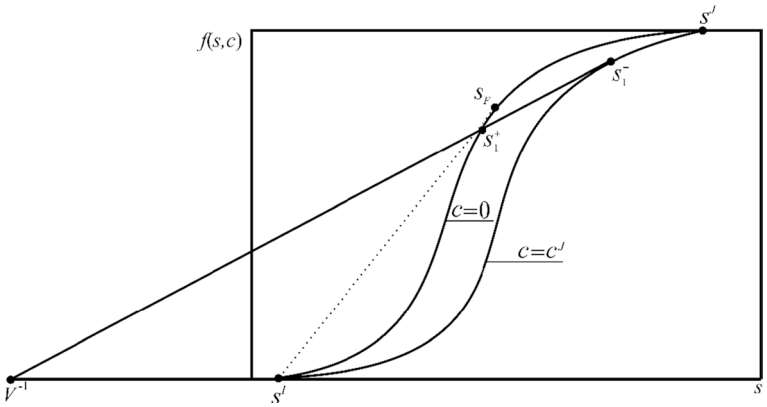

Fig. 1 Self-similar part of the solution in f–s plane

$$\mathrm{d}\varphi = f\mathrm{d}t - s\mathrm{d}x \tag{15}$$

and applying it in system (9) instead of time leads to the following partial differential equation for the polymer conservation

$$\frac{\partial c}{\partial x} + \frac{\partial a(c)}{\partial \varphi} = 0. \tag{16}$$

The initial and boundary conditions for Eq. (16) in the new coordinate system are given by

$$c(x, \varphi = 0) = 0 \quad \text{and} \quad c(x = 0, \varphi) = \begin{cases} c_n^J, & \varphi_{2n-2}^J \leq \varphi \leq \varphi_{2n-1}^J \\ 0, & \varphi_{2n-1}^J < \varphi < \varphi_{2n}^J \end{cases}, \quad n = 1, 2, \ldots, N \tag{17}$$

Following the same procedure for the first equation of the system (9), we obtain

$$\frac{\partial U}{\partial x} + \frac{\partial F(U, c)}{\partial \varphi} = 0 \tag{18}$$

where

$$U = \frac{1}{f(s, c)} \quad \text{and} \quad F(U, c) = -\frac{s}{f(s, c)} \tag{19}$$

and the initial and boundary conditions for Eq. (18) are

$$U(x, \varphi = 0) \to \infty \quad \text{and} \quad U(x = 0, \varphi) = 1. \tag{20}$$

3 Structure of the Solution

The solution of the problem (9)–(10) is built in three steps: solution of the auxiliary equation (Eq. (16)), solution of the lifting equation (Eq. (18)) and inverse mapping for time domain. Equations (16) and (18) are nonlinear hyperbolic equations, and their solution can be obtained using the method of characteristic (Whitham 1974; Logan 2008).

3.1 Auxiliary Equation Solution

Equation (16) models one-phase polymer transport in porous media (Rhee et al. 1989a). In quasilinear form it becomes

$$\frac{\partial c}{\partial x} + a'(c)\frac{\partial c}{\partial \varphi} = 0 \tag{21}$$

Therefore, along a characteristic curve ($\varphi(x)$) the polymer concentration is constant:

$$\frac{\mathrm{d}c(\varphi(x), x)}{\mathrm{d}x} = 0 \tag{22}$$

The trajectory of the characteristics is a straight line defined by

$$\frac{\mathrm{d}\varphi}{\mathrm{d}x} = a'(c) = \lambda(c) = \alpha(1+\beta c)^{-2} \tag{23}$$

The slope of a characteristic where the polymer concentration is zero ($c=0$) will be represented by $\lambda_0\left(\lambda_0 = \alpha\right)$ and if the concentration is c_n^J by $\lambda_n\left(\lambda_n = \lambda\left(c_n^J\right)\right)$. The speed ($\sigma$) of each characteristic wave is calculated by the inverse of Eq. (23):

$$\sigma_n = \left(1+\beta c_n^J\right)^2 \alpha^{-1}, \quad \sigma_0 = \sigma(0) = \alpha^{-1} \tag{24}$$

3.1.1 Rarefaction Waves

According to the boundary condition (Eq. (17)), at φ_{2n-1}^J a water slug is injected (no dissolved polymer). As the speed of the front of the polymer slug $\left(\sigma_n\right)$ is greater than its rear velocity $\left(\sigma_0\right)$, behind every polymer slug a rarefaction wave will appear. This is a centered wave at $\left(0, \varphi_{2n-1}^J\right)$, and its slope is given by

$$\frac{d\varphi}{dx} = \frac{\varphi - \varphi_{2n-1}^J}{x} = \frac{\alpha}{\left(1+\beta c_n(x,\varphi)\right)^2} \tag{25}$$

The polymer concentration at each rarefaction wave is determined by (Eq. (25)):

$$c_n(x,\varphi) = \frac{1}{\beta}\left(\sqrt{\frac{\alpha x}{\varphi - \varphi_{2n-1}^J}} - 1\right), \quad 0 \le c_n(x,\varphi) \le c_n^J \tag{26}$$

3.1.2 Shock Waves

The solution of the auxiliary equation also admits shock waves. The Rankine–Hugoniot condition for Eq. (16) is

$$\frac{\mathrm{d}\varphi}{\mathrm{d}x} = \frac{[a(c)]}{[c]} = \frac{a\left(c^+\right) - \left(c^-\right)}{c^+ - c^-} = \frac{1}{V} \tag{27}$$

where c^+ and c^- are the concentration values ahead and behind the discontinuity, respectively. Substituting the expression of the Langmuir isotherm into Eq. (27), we find the inverse of the shock speed in x–φ plane:

$$\frac{1}{V} = \frac{\alpha}{(1+\beta c^+)(1+\beta c^-)} \tag{28}$$

The speed of the shock is:

$$V = \frac{\left(1+\beta c^+\right)(1+\beta c^-)}{\alpha} \tag{29}$$

If c^+ and c^- are constant the inverse of the shock speed is also constant and will be denoted as $\frac{1}{V} = \tilde{\lambda}_{(n,r)} = \tilde{\lambda}\left(c_n^J, c_r^J\right)$.

Table 1 shows the shock paths obtained solving Eq. (27) to all possible c^+ and c^- combinations. Three types of shock may appear. In shock type I both concentrations behind and

Table 1 Shock types appearing in the solution of the auxiliary equation

Type	Jump conditions	Inverse of shock speed	Shock path
I	$\left(c^+ = 0,\ c^- = c_n^J\right)$ $\left(c^+ = c_n^J,\ c^- = c_{n+1}^J\right)$	$\frac{d\varphi}{dx} = \tilde{\lambda}_{(n,r)}$	$\varphi_{\mathrm{I}}^{(n,r)}(x) = \tilde{\lambda}_{(n,r)}\left(x - x_0\right) + \varphi_0$
IIa	$\left(c^+ = 0,\ c^- = c_n\right)$	$\frac{\mathrm{d}\varphi}{\mathrm{d}x} = \sqrt{\lambda_0\left(\frac{\varphi - \varphi_{2n-1}^J}{x}\right)}$	$\varphi_{\mathrm{IIa}}^{(n)}(x) = \left[\sqrt{\lambda_0}\left(\sqrt{x} - \sqrt{x_0}\right) + \sqrt{\varphi_0 - \varphi_{2n-1}^J}\right]^2 + \varphi_{2n-1}^J$
IIb	$\left(c^+ = c_n,\ c^- = c_n^J\right)$	$\frac{\mathrm{d}\varphi}{\mathrm{d}x} = \sqrt{\lambda_n\left(\frac{\varphi - \varphi_{2n-1}^J}{x}\right)}$	$\varphi_{\mathrm{IIb}}^{(n)}(x) = \left[\sqrt{\lambda_n}\left(\sqrt{x} - \sqrt{x_0}\right) + \sqrt{\varphi_0 - \varphi_{2n-1}^J}\right]^2 + \varphi_{2n-1}^J$
III	$\left(c^+ = c_{n+1},\ c^- = c_n\right)$	$\frac{\mathrm{d}\varphi}{\mathrm{d}x} = \sqrt{\frac{(\varphi - \varphi_{2n+1}^J)(\varphi - \varphi_{2n-1}^J)}{x}}$	$\sqrt{\frac{x}{x_0}} = \frac{\sqrt{\varphi_{\mathrm{III}}^{(n)}(x) - \varphi_{2n+1}^J} + \sqrt{\varphi_{\mathrm{III}}^{(n)}(x) - \varphi_{2n-1}^J}}{\sqrt{\varphi_0 - \varphi_{2n+1}^J} + \sqrt{\varphi_0 - \varphi_{2n-1}^J}}$

ahead of the shock are constant, this shock travels with constant speed and always appears at the front of any polymer slug. The shock type II results from the interaction between a rarefaction wave (Eq. (25)) with a shock type I. If the concentration ahead of the shock is zero $\left(c^+ = 0\right)$, its velocity decreases (shock type IIa). If the concentration behind the shock is constant $\left(c^- = c_n^J\right)$, its velocity increases (shock type IIb). The shock type III appears when two rarefaction waves intersect.

3.2 Lifting Equation

In quasilinear form Eq. (18) is given by

$$\frac{\partial U}{\partial x} + F'_U(U,c)\frac{\partial U}{\partial \varphi} = -F'_c(U,c)\frac{\partial c}{\partial \varphi} \tag{30}$$

where

$$F'_U(U,c) = \frac{\partial F(U,c)}{\partial U} \quad \text{and} \quad F'_c(U,c) = \frac{\partial F(U,c)}{\partial c}$$

Along the characteristic curves defined by

$$\frac{\mathrm{d}\varphi}{\mathrm{d}x} = F'_U(U,c) \tag{31}$$

we have

$$\frac{\mathrm{d}U(\varphi(x),x)}{\mathrm{d}x} = -F'_c(U,c)\frac{\partial c}{\partial \varphi}. \tag{32}$$

3.2.1 Rarefaction Waves

In regions of constant concentration, the right side of Eq. (32) is zero, therefore U is constant on the characteristics curves. Thus, the characteristics are straight lines. In regions where the concentration changes, Eqs. (31) and (32) must be solved simultaneously to obtain the characteristic curves and the value of U.

3.2.2 Shock Waves

The concentration shock path in the solution of Eq. (18) is obtained in the solution of the auxiliary equation (Eq. (16)), and also obeys the Rankine–Hugoniot conditions:

$$\frac{\mathrm{d}\varphi}{\mathrm{d}x} = \frac{[F(U,c)]}{[U]} = \frac{F\left(U^+, c^+\right) - F(U^-, c^-)}{U^+ - U^-}. \tag{33}$$

3.3 Inverse Mapping

After the auxiliary and lifting equations are solved, the next step is the inverse mapping of the solution from (x, φ)-plane to (x, t)-plane. This procedure is performed for rarefaction and shock waves, substituting relations (19) into Eq. (15) and integrating the resulting equation from $\left(x_0, \varphi_0\right)$ to (x, φ):

$$t(x) = t_0 + \int_{\varphi_0}^{\varphi} U\left(x, \varphi'\right)\mathrm{d}\varphi' - \int_{x_0}^{x} F\left(U\left(x', \varphi\right), c\left(x', \varphi\right)\right)\mathrm{d}x' \tag{34}$$

Applying Eq. (31) (rarefaction waves) into Eq. (34) we obtain

$$t(x) = t_0 + \int_{x_0}^{x} \left[UF'_U(U,c) - F(U,c)\right]\mathrm{d}x \tag{35}$$

and applying Eq. (33) (shock waves) into Eq. (34) we obtain

$$t(x) = t_0 + \int_{x_0}^{x} \left(U^+[F][U]^{-1} - F^+\right)\mathrm{d}x = t_0 + \int_{x_0}^{x} \left(U^-[F][U]^{-1} - F^-\right)\mathrm{d}x \tag{36}$$

where $F^{\pm} = F(U^{\pm}, c^{\pm})$.

Equations (35) and (36) allow us to calculate $t(x)$ along any characteristic curve $\varphi(x)$ and shock path.

The saturation at each characteristic and constant region is obtained from the following expression

$$s = -\frac{F(U,c)}{U}. \tag{37}$$

4 Example of a Particular Solution

The methodology developed to build the solution of system (9) will be applied to solve a particular case of water alternating polymer (WAP) injection subject to the following initial and boundary conditions:

$$t=0:\begin{cases} s=s^J \rightarrow f(s,c)=0 \\ c=0 \end{cases} \quad \text{and} \quad x=0:\begin{cases} s=s^J \rightarrow f(s,c)=1 \\ c(t)=\begin{cases} c^J, & t_{2n-2}^J \le t \le t_{2n-1}^J \\ 0, & t_{2n-1}^J < t < t_{2n}^J \end{cases}, n=1,2 \end{cases} \tag{38}$$

4.1 Solution of the Auxiliary Equation

As the polymer concentration of both slugs is the same $\left(c_1^J = c_2^J = c^J\right)$, at the front of the first slug there is a type I shock concentration (Table 1) ($c^J \xrightarrow{D_c} 0$), the trajectory of this shock is defined by the straight line $\varphi_{\mathrm{I}}^{(1,0)} = \tilde{\lambda}_{1,0} x$. Note that the concentration of both polymer slugs is the same $\left(c_1^J = c_2^J = c^J\right)$. Behind this slug there is a family of constant concentration rarefaction waves where the concentration changes from c^J with speed σ_1 to 0 with speed σ_0. The polymer concentration at each rarefaction wave behind the first slug can be calculated through (Fig. 2)

$$c_1(x,\varphi) = \frac{1}{\beta}\left(\sqrt{\frac{\alpha x}{\varphi - \varphi_1^J}} - 1\right) \tag{39}$$

The first slug is displaced by water until φ_2^J, at this point the injection of second polymer slug begins. At point (1), defined by the intersection of the characteristic $\varphi = \lambda_1 x + \varphi_1^J$ and the shock $\varphi_{\mathrm{I}}^{(1,0)}$ (Fig. 2)

$$\left(x_1, \varphi_1\right) = \left(\frac{\varphi_1^J}{\tilde{\lambda}_{1,0} - \lambda_1}, \frac{\tilde{\lambda}_{1,0}\varphi_1^J}{\tilde{\lambda}_{1,0} - \lambda_1}\right) = \left(\frac{\left(1+\beta c_1^J\right)^2}{\alpha\beta c_1^J}\varphi_1^J, \frac{1+\beta c_1^J}{\beta c_1^J}\varphi_1^J\right) \tag{40}$$

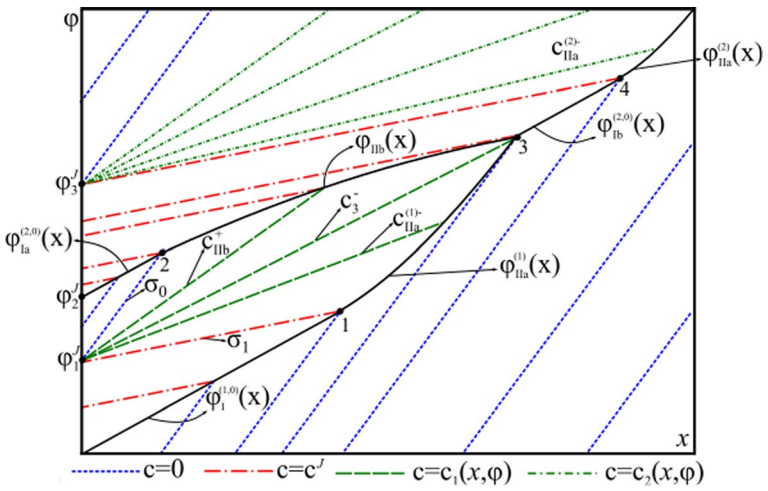

Fig. 2 Auxiliary system solution (characteristic diagram)

a decreasing speed shock (Type IIa) develops, the trajectory of this shock is given by

$$\varphi_{\mathrm{IIa}}^{(1)}(x)=\left[\sqrt{\lambda_0}\left(\sqrt{x}-\sqrt{x_1}\right)+\sqrt{\varphi_1-\varphi_1^J}\right]^2+\varphi_1^J. \tag{41}$$

Ahead of the second slug, there is also a discontinuity ($c^J \xrightarrow{D_c} 0$), its trajectory is given by the straight line $\varphi_{\mathrm{I}}^{(2,0)}=\tilde{\lambda}_{2,0}x+\varphi_2^J$. At point

$$\left(x_2,\varphi_2\right)=\left(\frac{\varphi_2^J-\varphi_1^J}{\lambda_0-\tilde{\lambda}_{2,0}},\frac{\varphi_2^J\lambda_0-\varphi_1^J\tilde{\lambda}_{2,0}}{\lambda_0-\tilde{\lambda}_{2,0}}\right)=\left(\frac{1+\beta c_1^J}{\alpha\beta c_2^J}\varphi_1^J,\frac{\left(1+\beta c_1^J\right)\varphi_2^J-\varphi_1^J}{\beta c_2^J}\right) \tag{42}$$

the shock ahead of the second slug intersects the characteristic $\varphi=\lambda_0 x+\varphi_1^J$ (last characteristic of the rarefaction wave behind the first polymer slug), and a shock-rarefaction wave interaction begins. At this point the front of the second slug travels with increasing speed (shock type IIb). The path of this shock $\left(c^-=c^J,\ c^+=c_1(x,\varphi)\right)$ in (x,φ)-plane is given by

$$\varphi_{\mathrm{IIb}}(x)=\left[\sqrt{\lambda_2}\left(\sqrt{x}-\sqrt{x_2}\right)+\sqrt{\varphi_2-\varphi_1^J}\right]^2+\varphi_1^J \tag{43}$$

The shock $\varphi_{\mathrm{IIa}}^{(1)}$ intercepts shock φ_{IIb} (Fig. 2) at point (3):

$$\left(x_3,\varphi_3\right)=\left(\frac{B\sqrt{B^2-4AC}-2AC+B}{2A},\left[\sqrt{\lambda_2}\left(\sqrt{x_3}-\sqrt{x_2}\right)+\sqrt{\varphi_2-\varphi_1^J}\right]^2+\varphi_1^J\right) \tag{44}$$

where

$$A=\lambda_2-\lambda_0$$
$$B=2\left(\sqrt{\lambda_2\left(\varphi_2-\varphi_1^J\right)}-\sqrt{\lambda_0\left(\varphi_1-\varphi_1^J\right)}+\lambda_0\sqrt{x_1}-\lambda_2\sqrt{x_2}\right)$$
$$C=\lambda_2x_2-\lambda_0x_1-2\left[\sqrt{\lambda_2x_2\left(\varphi_2-\varphi_1^J\right)}-\sqrt{\lambda_0x_1\left(\varphi_1-\varphi_1^J\right)}\right]+\varphi_2-\varphi_1$$

Along the left side of the shock path $\varphi_{\mathrm{IIa}}^{(1)}$ the polymer concentration $\left(c_{\mathrm{IIa}}^{(1)-}\right)$ decreases from c^J at $\left(x_1,\varphi_1\right)$ to c_3^- at $\left(x_3,\varphi_3\right)$ and along the right side of curve φ_{IIb} the polymer concentration $\left(c_{\mathrm{IIb}}^+\right)$ increases from zero at $\left(x_2,\varphi_2\right)$ to c_3^- at $\left(x_3,\varphi_3\right)$. Concentration c_3^- is determined from Eq. (26):

$$c_3^-=\frac{1}{\beta}\left(\sqrt{\frac{\alpha x_3}{\varphi_3-\varphi_1^J}}-1\right) \tag{45}$$

At point (3) another type I concentration shock appears. Its trajectory is given by $\varphi_{\mathrm{I}}^{(2,0)}(x)=\tilde{\lambda}_{2,0}\left(x-x_3\right)+\varphi_3$, and it travels at constant speed. At point

$$\left(x_4,\varphi_4\right)=\left(\frac{\varphi_3-\varphi_3^J-\tilde{\lambda}_{2,0}x_3}{\lambda_1-\tilde{\lambda}_{2,0}},\frac{\lambda_1\varphi_3-\tilde{\lambda}_{2,0}\left(\lambda_1x_3+\varphi_3^J\right)}{\lambda_1-\tilde{\lambda}_{2,0}}\right) \tag{46}$$

the rarefaction wave behind the second slug overtakes the shock $\varphi_{\mathrm{I}}^{(2,0)}$. The trajectory of this wave (shock-rarefaction interaction) is given by (shock type IIa)

$$\varphi_{\mathrm{IIa}}^{(2)}(x) = \left[\sqrt{\lambda_0}\left(\sqrt{x} - \sqrt{x_4}\right) + \sqrt{\varphi_4 - \varphi_3^J}\right]^2 + \varphi_3^J \tag{47}$$

Behind the curve $\varphi_{\mathrm{IIa}}^{(2)}$ the polymer concentration $\left(c_{\mathrm{IIa}}^{(2)-}\right)$ decreases from c^J at (x_4, φ_4) to 0 when $(x_3, \varphi_3) \to \infty$. The polymer concentration changes along this wave (second rarefaction wave) according to

$$c_2(x, \varphi) = \frac{1}{\beta}\left(\sqrt{\frac{\alpha x}{\varphi - \varphi_3^J}} - 1\right) \tag{48}$$

At $\left(0, \varphi_3^J\right)$ the second slug is displaced by water.

4.2 Solution of the Lifting Equation

Although the original system is decoupled, the lifting equation can be solved only after the auxiliary problem solution. Figure 3 shows the solution in (F, U)-plane for $\varphi < \varphi_1^J$ (self-similar solution), composed by a rarefaction wave from $U = 1$ to U_1^-; followed by a shock wave linking U_1^- to U_1^+; then there is a rarefaction wave from U_1^+ to U_f; and finally a shock wave connecting the initial condition.

Interactions of waves of different families begin when $\varphi > \varphi_1^J$. Figure 4 shows the solution of the lifting equation in the $x - \varphi$ diagram. A U-rarefaction centered at point $(0, 0)$ appears in region I; its characteristic slopes are given by

$$\frac{\varphi}{x} = F'_U\left(U_{\#}^{(1)}, c^J\right), \quad 1 < U_{\#}^{(1)} < U_1^+. \tag{49}$$

In region III both U and c change along characteristics. On the characteristic curves beginning at $\varphi = \lambda_1 x + \varphi_1^J$; U changes from $U_{\#}^{(1)}$ to $U_*^{(1)}$ on the curve $\varphi = \lambda_0 x + \varphi_1^J$ if $\varphi < \varphi_2$; or to $U_{\mathrm{IIb}}^{(1)+}$ on the curve $\varphi_{\mathrm{IIb}}(x)$ if $\varphi_2 < \varphi < \varphi_3$ (Fig. 4).

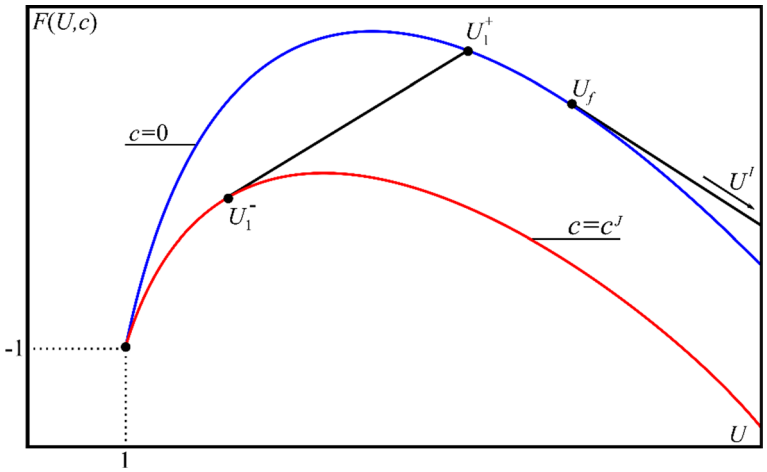

Fig. 3 Self-similar solution of the lifting equation in (F, U)-plane

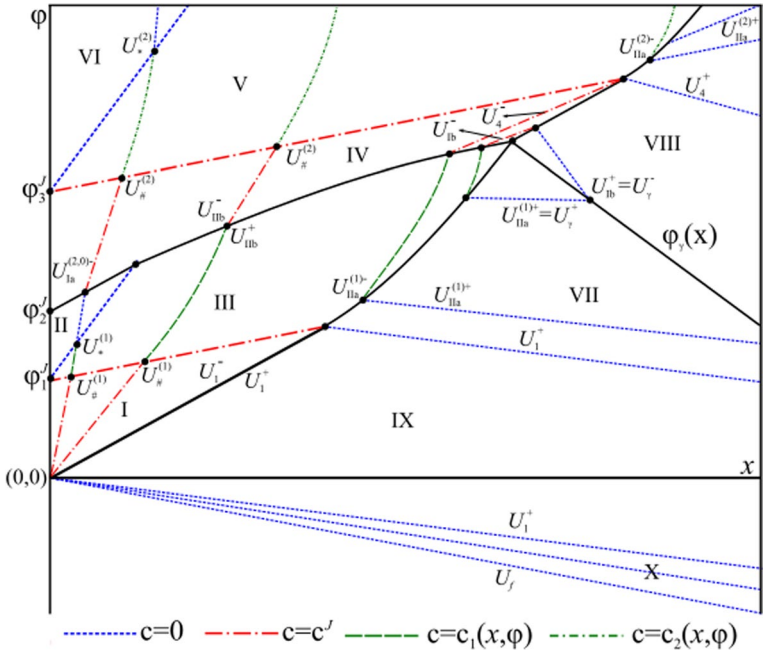

Fig. 4 Solution of the lifting equation (characteristic diagram)

In region II, $c = 0$ and U is constant $\left(U_*^{(1)}\right)$, the slope of each characteristic is $F'_U\left(U_*^{(1)} = U_{\text{Ia}}^{(2,0)+}, 0\right)$. This characteristic interacts with the shock $\varphi_{\text{Ia}}^{(2,0)}$; where $U^- = U_{\text{Ia}}^{(2,0)-} = U_{\#}^{(2)}$, and $U^+ = U_{\text{Ia}}^{(2,0)+} = U_*^{(1)}$ (Fig. 5a). In region IV, $c = c^J$ and U is constant. Across the curve $\varphi_{\text{IIb}}(x)$, there is a concentration shock where $U^- = U_{\text{IIb}}^-$ lies on the curve $F\left(U, c^J\right)$. and $U^+ = U_{\text{IIb}}^+$ lies on the fractional flow curve $F\left(U, c_{\text{IIb}}^+\right)$ (Fig. 5b). The slope of the U-characteristics in region IV is $F'_U\left(U, c^J\right)$. In the region where U changes between U_4^- and $U_{3\text{b}}^-$ (Figs. 4 and 5), these characteristics will catch up the shock curve $\varphi_{\text{Ib}}^{(2,0)}(x)$ (Fig. 2).

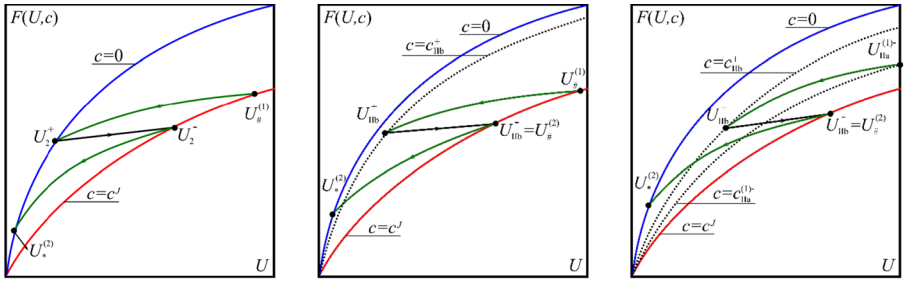

(a) Shock between regions II and IV **(b)** Shock between regions III and IV **(c)** Shock between end of region III and region IV

Fig. 5 Solution trajectory in F–U plane (lifting equation)

At point 3, U_{3a}^{-} jumps to U_{3a}^{+} (slope $\tilde{\lambda}\left(c_3^{-}, 0\right)$) and to U_{3b}^{-} (slope $\tilde{\lambda}\left(c_3^{-}, c^J\right)$) (Figs. 4 and 6a); and at point $\left(U_{3b}^{-},\ F\left(U_{3b}^{-}, c^J\right)\right)$ there is another jump to $\left(U_{3b}^{+},\ F\left(U_{3b}^{+}, 0\right)\right)$ with slope $\tilde{\lambda}\left(c^J, 0\right)$ (Figs. 4 and 6a). Since the speed of the characteristic carrying U_{3b}^{+} is greater than the speed of the characteristic carrying U_{3a}^{+}, the simple wave $\left(U_{Ib}^{+},\ c=0\right)$; where $U_4^{+} < U_{Ib}^{+} < U_{3b}^{+}$; arising from the curve $\varphi_{Ib}^{(2,0)}(x)$ will intercept the simple wave $\left(U_{IIa}^{(1)+},\ c=0\right)$; where $U_{3a}^{+} < U_{IIa}^{(1)+} < U_1^{+}$; arising from the curve $\varphi_{IIa}^{(1)}(x)$ (Fig. 4). This interaction starts at point 3 and takes place along the shock curve $\varphi_\gamma(x)$; where $U_\gamma^{+} = U_{IIa}^{(1)+}$ and $U_\gamma^{-} = U_{Ib}^{+}$ (Figs. 4,6a and 6b); its trajectory is given by (see details in "Appendix"):

$$\frac{\mathrm{d}\varphi_\gamma}{\mathrm{d}x} = \frac{F\left(U_\gamma^{-}, 0\right) - F\left(U_\gamma^{+}, 0\right)}{U_\gamma^{-} - U_\gamma^{+}}. \tag{50}$$

If all characteristics arising from curve $\varphi_{IIa}^{(1)}(x)$ intercept the characteristics arising from curve $\varphi_{Ib}^{(2,0)}(x)$, the characteristics of region VIII will interact with constant state U_1^{+} (Fig. 6c), where $U_\gamma^{+} = U_1^{+}$.

On the other hand, if only part of the characteristics arising from the curve $\varphi_{IIa}^{(1)}(x)$ intercepts the characteristics arising from the curve $\varphi_{Ib}^{(2,0)}(x)$, the remaining characteristics will interact with the characteristics arising from the curve $\varphi_{IIa}^{(2)}(x)$ (Fig. 6d).

The solution in regions V, VII and VIII is analogous to solution in region II and the solution in region V is analogous to solution in region III.

Along the curves $\varphi_{IIa}^{(n)}(x)\left(c^{+}=0,\ c^{-}=c_n(x,\varphi)\right)$, the shock speed is equal to the characteristic speed (Fig. 7):

$$F'_U\left(U_{IIa}^{(n)-}, c_{IIa}^{(n)-}\right) = \frac{F\left(U_{IIa}^{(n)-}, c_{IIa}^{(n)-}\right) - F\left(U_{IIa}^{(n)+}, 0\right)}{U_{IIa}^{(n)-} - U_{IIa}^{(n)+}} \tag{51}$$

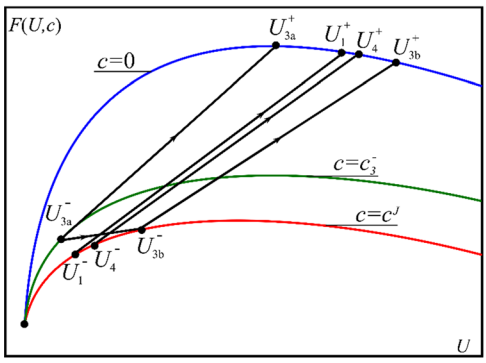

(a) Jump between regions III and VII; and between regions IV and VIII

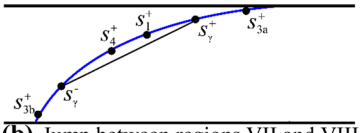

(b) Jump between regions VII and VIII

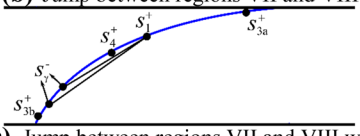

(c) Jump between regions VII and VIII where $U_\gamma^{+} = U_1^{+}$

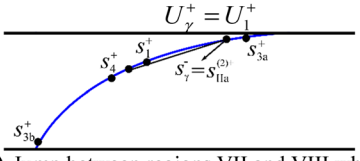

(d) Jump between regions VII and VIII where $U_\gamma^{-} = U_{IIa}^{(2)+}$

Fig. 6 Jump conditions for $U\left(U_\gamma^{\pm}\right)$

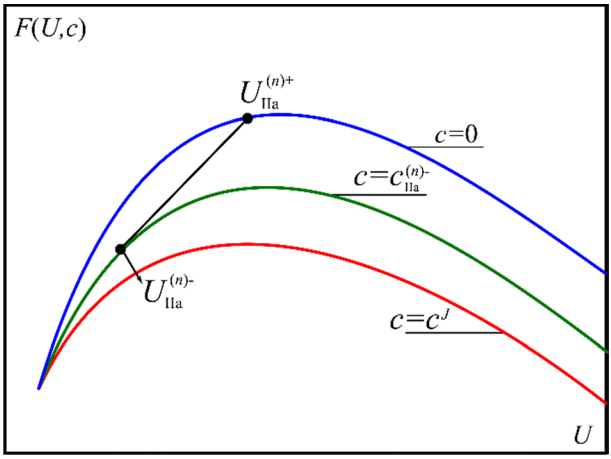

Fig. 7 Jump conditions for $U_{IIa}^{(n)\pm}$

4.3 Inverse Mapping

The final part of the solution is the inverse mapping from (x, φ)-plane to (x, t)-plane. So, the characteristic diagram presented in Fig. 4 is mapped in x–t domain using the relations given by Eqs. (35) and (36) (Fig. 8). In constant concentration $\left(c = 0 \text{ or } c = c^J\right)$ regions, Eq. (35) reduces to

$$t(x) = t_0 + \left[UF'_U(U,c) - F(U,c)\right]\left(x - x_0\right) \tag{52}$$

The solution for $t < t_1^J$ is presented in Sect. 2.1. For $t > t_1^J$ the discontinuity in the boundary condition leads to interactions between rarefactions and shocks waves.

Interactions between an s-wave and a c-wave appear in regions III and VI (Fig. 8). In other regions with constant concentration, we have

$$\frac{x - x'}{t - t'} = \left[UF'_U(U,c) - F(U,c)\right]^{-1} = f'_s(s,c) \text{ or } \frac{x}{t} = \left[UF'_U(U,c) - F(U,c)\right]^{-1} = f'_s(s,c) \tag{53}$$

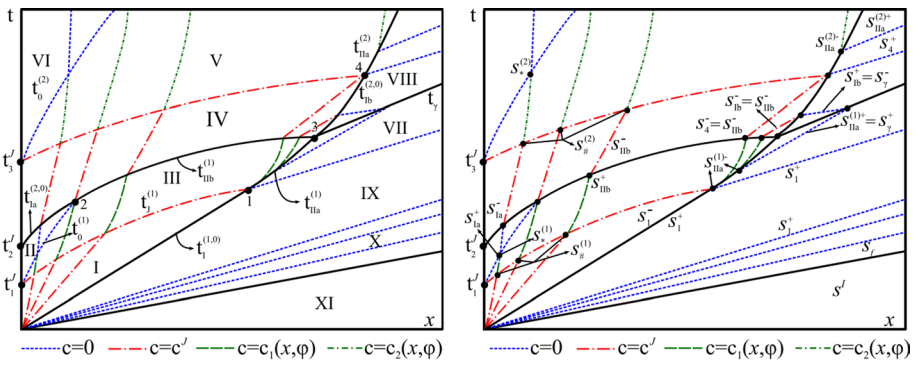

(a) Shock and rarefaction waves **(b)** Conditions ahead and behind the shocks

Fig. 8 Characteristic diagram in x–t domain

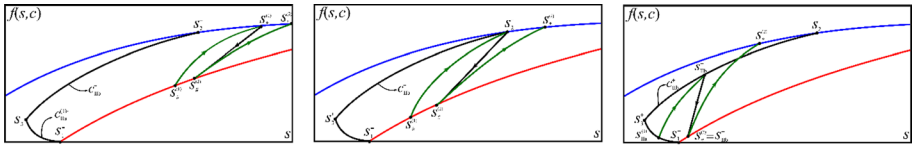

(a) Shock between regions II and IV **(b)** Shock between regions III and IV **(c)** Shock between end of region III and region IV

Fig. 9 Solution trajectory in the *f*–*s* plane

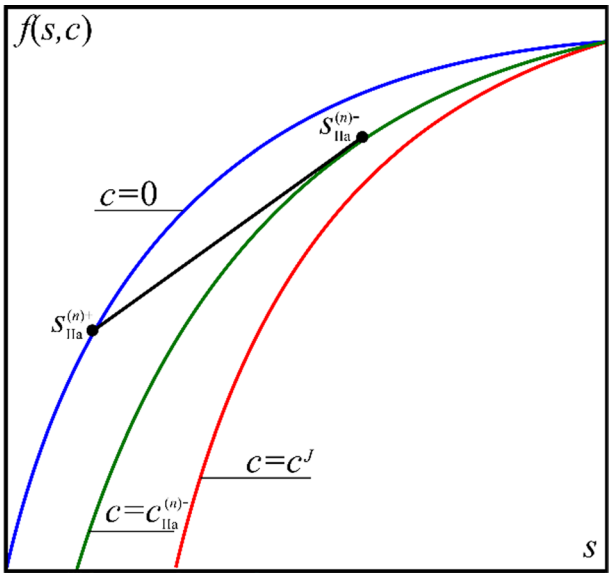

Fig. 10 Jump conditions for $s_{\mathrm{IIa}}^{(n)+}$

where (x', t') is the characteristic initial point.

After the coordinate transformation, the straight lines $\varphi = \lambda_n x + \varphi_{2n+1}^J$ and $\varphi = \lambda_0 x + \varphi_{2n+1}^J$ are mapped onto the curves $t_J^{(n)}(x)$ and $t_0^{(n)}(x)$, respectively (Fig. 8a). For $0 < x < x_2$ the water saturation increases from $s_{\#}^{(1)}$ on the curve $t_J^{(1)}(x)$ to $s_*^{(1)}$ on the curve $t_0^{(1)}(x)$ (Figs. 8b and 9a); for $x_2 < x < x_3$ the saturation increases up to s_{IIb}^+ on curve $t_{\mathrm{IIb}}(x)$, where $s_{\mathrm{IIb}}^+ > s_{\mathrm{IIb}}^- = s_{\#}^{(2)}$ (Figs. 8b and 9b). The shock trajectory ahead of the second slug is mapped onto plane x–t through the curve $t_{\mathrm{Ia}}^{(2,0)}(x)$ (with increasing speed), where $s_{\mathrm{Ia}}^+ = s_*^{(1)} > s_{\mathrm{Ia}}^- = s_{\#}^{(2)}$ (Figs. 8b and 9a).

Along the shock path $t_{\mathrm{IIa}}^{(n)}(x)$; $s_{\mathrm{IIa}}^{(n)+} > s_{\mathrm{IIa}}^{(n)-}$ (Fig. 10), the velocity of this shock is equal to the characteristic speed behind the discontinuity and decreases with time. When $t \to \infty$, $s_{\mathrm{IIa}}^{(2)\pm} \to s_\infty$, where s_∞ lies on the curve $f(s, 0)$.

All constant saturation characteristics in region IV, where saturation is smaller than s_4^-, intercept the front of the polymer slug $t_{\mathrm{Ib}}^{(2,0)}(x)$ (Fig. 8b). In this shock $s_{\mathrm{Ib}}^+ > s_{\mathrm{Ib}}^-$.

The velocity of the characteristics in region VII is given by (Figs. 8a, 8b and 11a)

$$\frac{\mathrm{d}x}{\mathrm{d}t} = f_s'(s, 0), \quad s_1^+ < s = s_{\mathrm{IIa}}^{(1)+} < s_{3\mathrm{a}}^+ \tag{54}$$

and in region VIII by (Figs. 8a, 8b and 11a)

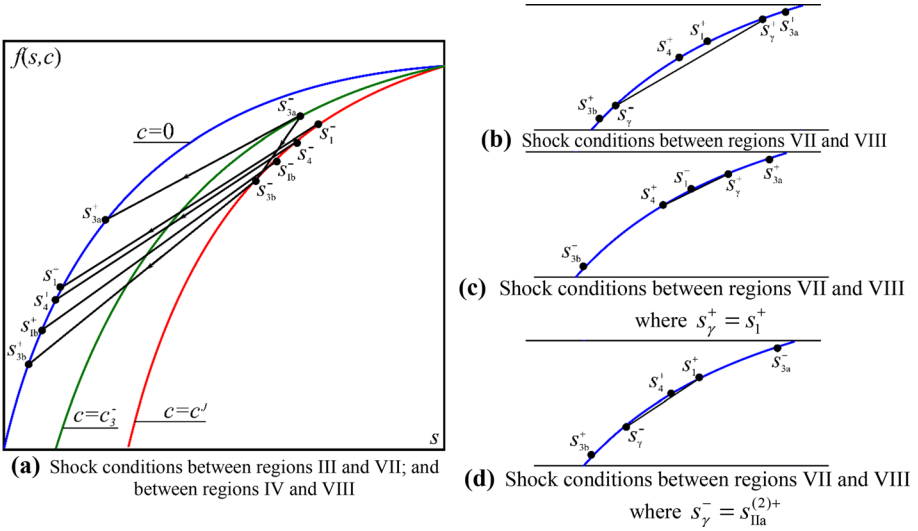

Fig. 11 Shock conditions for $s_\gamma^{\pm}$

$$\frac{\mathrm{d}x}{\mathrm{d}t} = f_s'(s,0), \quad \begin{array}{l} s_{3\mathrm{b}}^+ < s = s_{\mathrm{Ib}}^+ < s_4^+, \ \ (t-t_4) < f_s'\left(s_4^+,0\right)(x-x_4) \\ s_4^+ < s = s_{\mathrm{IIa}}^{(2)+} < s_\infty, \ \ (t-t_4) > f_s'\left(s_4^+,0\right)(x-x_4) \end{array} \tag{55}$$

The velocity of characteristics in region VIII is greater than the velocity of characteristics in region VII, since the value of saturations in region VII is greater than in region VIII. Therefore, these waves intercept along the shock path $t_\gamma(x)$ (Fig. 8a), obtained through Eq. (36). Along this shock path $s_\gamma^- < s_\gamma^+$ (Fig. 11b). As described previously, two different waves interaction structure between the rarefaction waves of regions VII and VIII may appear. One possibility is that the characteristics arising from curve $t_{\mathrm{IIa}}^{(1)}(x)$ interact with characteristics arising from curves $t_{\mathrm{Ib}}^{(2,0)}(x)$ and $t_{\mathrm{IIa}}^{(2)}(x)$ (Fig. 11c); in the other scenario all characteristics arising from curve $t_{\mathrm{IIa}}^{(1)}(x)$ interact with waves arising from curve $t_{\mathrm{Ib}}^{(2,0)}(x)$ (Fig. 11d). In the last case, a new shock appears, resulting from the interaction between the characteristics carrying s_1^+ and the discontinuity $t_\gamma(x)$, and its speed is given by

$$\frac{\mathrm{d}x}{\mathrm{d}t} = \frac{f\left(s_\gamma^-,0\right) - f\left(s_1^+,0\right)}{s_\gamma^- - s_1^+} \tag{56}$$

It is important to note that, although the polymer concentration is constant ahead and behind ($c^- = c^J$ and $c^+ = 0$) the trajectories of the polymer slug front ($t_{\mathrm{I}}^{(1,0)}(x)$, $t_{\mathrm{Ia}}^{(2,0)}(x)$ and $t_{\mathrm{Ib}}^{(2,0)}(x)$); only shock $t_{\mathrm{I}}^{(1,0)}(x)$ travels with constant speed; the velocity of $t_{\mathrm{Ia}}^{(2,0)}(x)$ and $t_{\mathrm{Ib}}^{(2,0)}(x)$ is increasing and decreasing, respectively.

Table 2 shows the velocity of all shocks present in the solution of problem (9)–(10) in the x–t domain and the saturation value ahead and behind of each discontinuity.

Figure 12 presents the solution for this particular problem in f–s plane and Fig. 13 shows the respective saturation and concentration profiles during each slug injection (water and polymer) and between the end of the slug injection and the point of shocks intersection

Table 2 Shock waves in x–t plane solution

Shock speed (dx/dt)	Shock path	Saturation ahead of shock	Saturation behind of shock
$\frac{f(s^+_{\mathrm{IIb}},c^+_{\mathrm{IIb}})}{s^+_{\mathrm{IIb}}+\tilde{\lambda}(c^+_{\mathrm{IIb}},c^J)} = \frac{f(s^-_{\mathrm{IIb}},c^J)}{s^-_{\mathrm{IIb}}+\tilde{\lambda}(c^+_{\mathrm{IIb}},c^J)}$	$t_{\mathrm{IIb}}(x)$	$s_2^+ < s^+_{\mathrm{IIb}} < s^-_{3a}$	$s_2^- < s^-_{\mathrm{IIb}} < s^-_{3\mathrm{b}}$
$\frac{f\left(s^{(2,0)+}_{\mathrm{Ia}},0\right)}{s^{(2,0)+}_{\mathrm{Ia}}+\tilde{\lambda}(0,c^J)} = \frac{f\left(s^{(2,0)-}_{\mathrm{Ia}},c^J\right)}{s^{(2,0)-}_{\mathrm{Ia}}+\tilde{\lambda}(0,c^J)}$, $\pi = a,\ b$	$t^{(2,0)}_{\mathrm{Ia}}(x)$	$s^J < s^+_{\mathrm{Ia}} < s_2^+$	$s^J < s^-_{\mathrm{Ia}} < s_2^-$
	$t^{(2,0)}_{\mathrm{Ib}}(x)$	$s^+_{3\mathrm{b}} < s^+_{\mathrm{Ib}} < s_4^+$	$s^-_{3\mathrm{b}} < s^-_{\mathrm{Ib}} < s_4^-$
$\frac{f\left(s^{(n)+}_{\mathrm{IIa}},0\right)}{s^{(n)+}_{\mathrm{IIa}}+\tilde{\lambda}\left(c^{(n)+}_{\mathrm{IIa}},0\right)} = \frac{f\left(s^{(n)-}_{\mathrm{IIa}},c^{(n)-}_{\mathrm{IIa}}\right)}{s^{(n)-}_{\mathrm{IIa}}+\tilde{\lambda}\left(c^{(n)-}_{\mathrm{IIa}},0\right)} = f'_s\left(s^{(n)-}_{\mathrm{IIa}}, c^{(n)-}_{\mathrm{IIa}}\right)$, $n = 1,\ 2$	$t^{(1)}_{\mathrm{IIa}}(x)$	$s_1^+ < s^{(1)+}_{\mathrm{IIa}} < s^+_{3a}$	$s^-_{3a} < s^{(1)-}_{\mathrm{IIa}} < s_1^-$
	$t^{(2)}_{\mathrm{IIa}}(x)$	$s_4^+ < s^{(2)+}_{\mathrm{IIa}} < s_\infty$	$s_4^- < s^{(2)-}_{\mathrm{IIa}} < s_\infty$
$\frac{f\left(s^+_\gamma,0\right)-f\left(s^-_\gamma,0\right)}{s^+_\gamma+s^-_\gamma}$	$t_\gamma(x)$	$s^+_{3\mathrm{b}} < s^+_\gamma < s_4^+$	$s^-_{3\mathrm{b}} < s^-_\gamma < s_4^-$

(points 1, 2, 3 and 4 shown in Fig. 8a). Table 3 shows the waves sequences for all solution profiles. Besides the notation introduced in Sect. 2.1 to denote shock and rarefaction waves, the symbol $\xrightarrow{R_c}$ stands for the trajectory of an s-wave and a c-wave interaction wave.

5 Validation

In this section we compare our solution to numerical results using the finite volume method.

Water fractional flow was calculated using the following analytical expression:

$$f(s,c) = \frac{2s^2}{2s^2 + (1+c)(1-s)^2} \tag{57}$$

and the adsorption isotherm is given by

$$a(c) = \frac{c}{1+5c} \tag{58}$$

Discretizing system of Eqs. (9) using an upwind finite volume method (LeVeque 2002) leads to

$$s_i^{n+1} = s_i^n - \frac{\Delta t}{\Delta x}\left(f_i^n - f_{i-1}^n\right) \tag{59}$$

$$M_i^{n+1} = M_i^n - \frac{\Delta t}{\Delta x}\left(F_i^n - F_{i-1}^n\right) \tag{60}$$

where $M = cs + a(c)$ and $F = cf$.

After calculating M_i^{n+1}, it is possible to find c_i^{n+1} solving the following transcendental equation

$$(cs)_i^{n+1} + a\left(c_i^{n+1}\right) - M_i^{n+1} = 0 \tag{61}$$

Equation (61) was solved using Newton´s method.

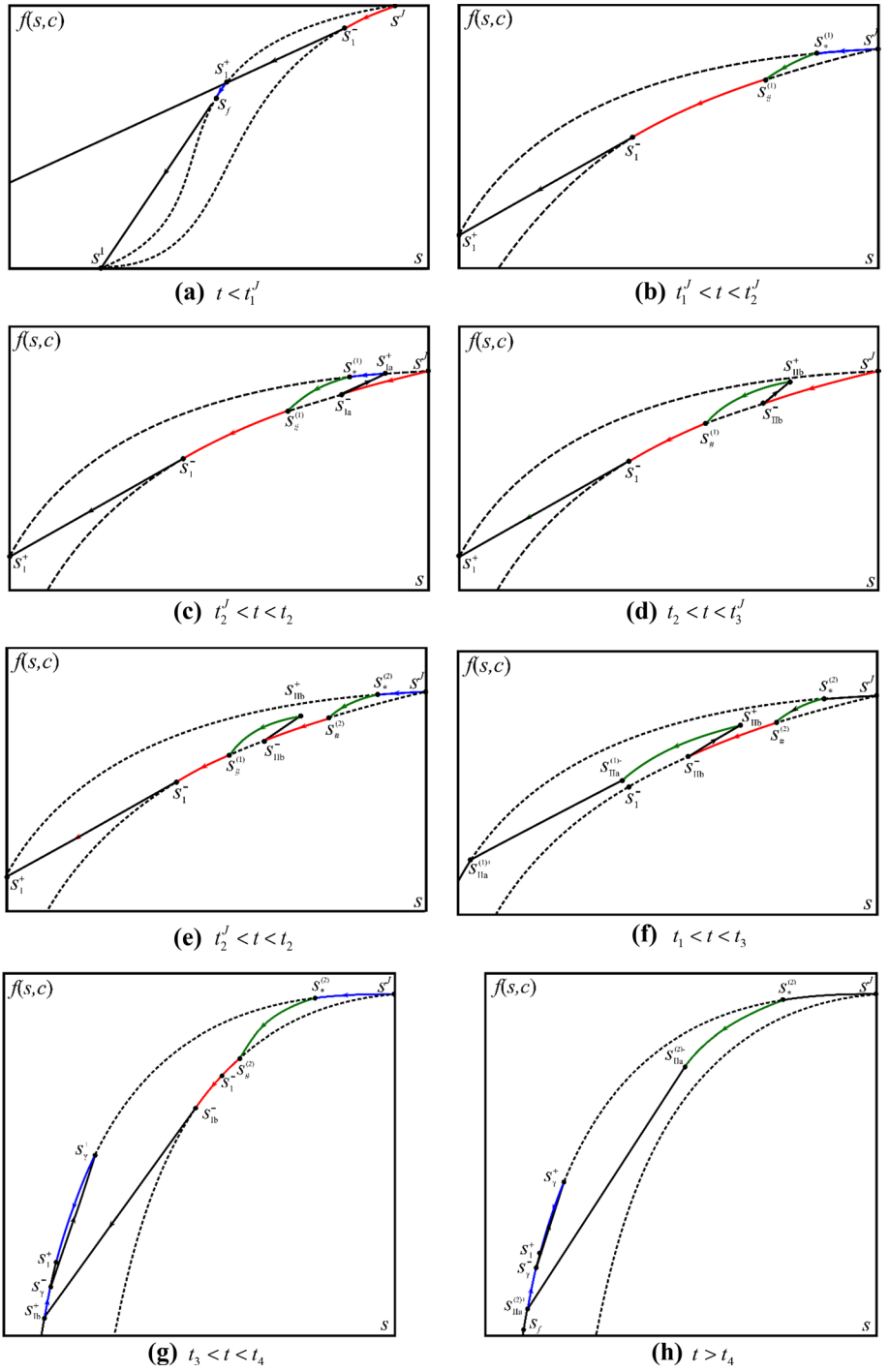

Fig. 12 Solution trajectory in *f*–*s* plane

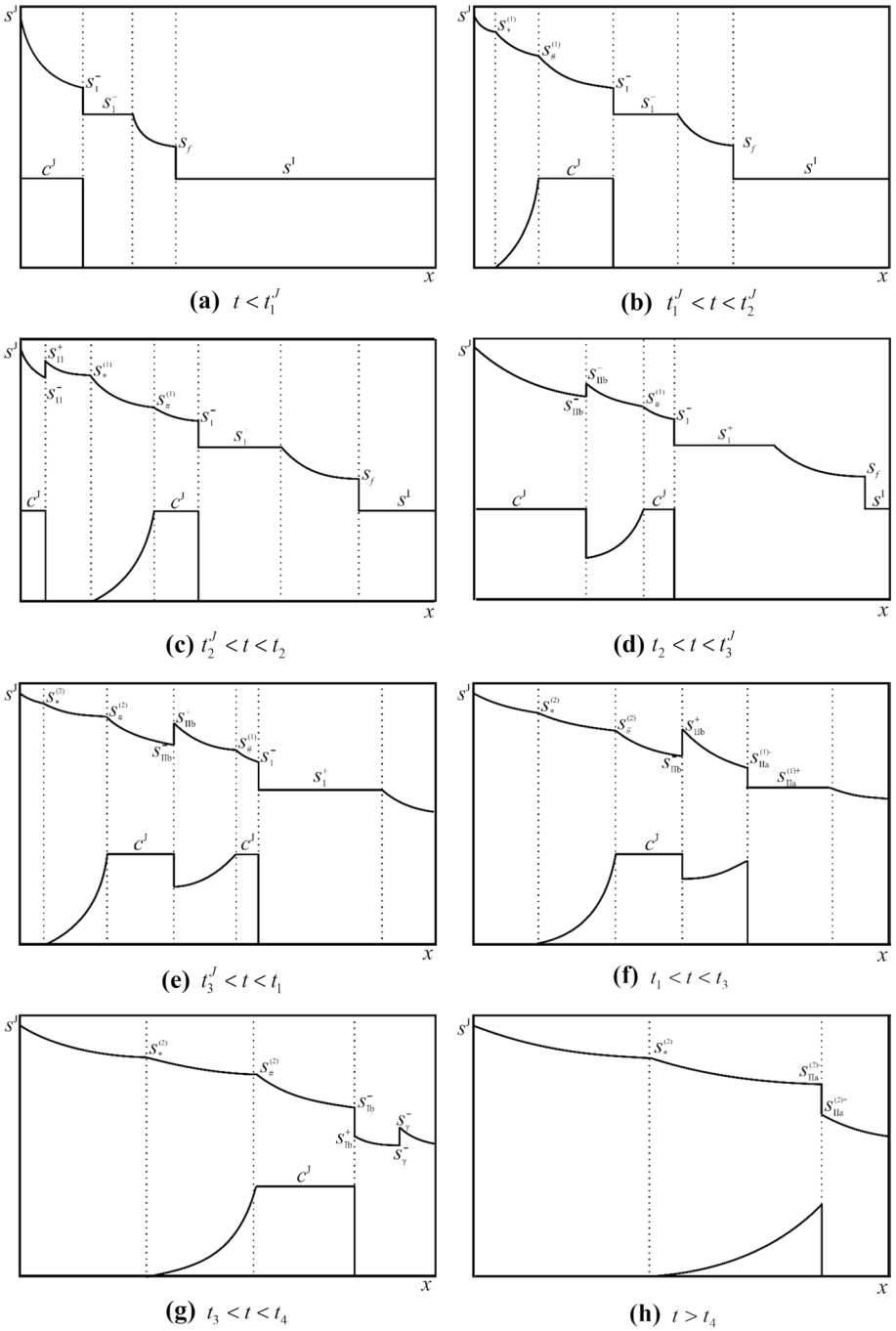

Fig. 13 Solution profile (saturation and concentration)

Table 3 Waves sequences of the solution profiles

Time range	Solution path
$t < t_1^J$	$J \xrightarrow{R_s^J} s_1^- \xrightarrow{D_c} s_1^+ \xrightarrow{R_s^0} s_F \xrightarrow{D_s} I$
$t_1^J < t < t_2^J$	$J \xrightarrow{R_s^0} s_*^{(1)} \xrightarrow{D_c} s_\#^{(1)} \xrightarrow{R_s^J} s_1^- \xrightarrow{D_c} s_1^+ \xrightarrow{R_s^0} s_F \xrightarrow{D_s} I$
$t_2^J < t < t_2$	$J \xrightarrow{R_s^J} s_{\mathrm{I1}}^- \xrightarrow{D_c} s_{\mathrm{I1}}^+ \xrightarrow{R_s^0} s_*^{(1)} \xrightarrow{D_c} s_\#^{(1)} \xrightarrow{R_s^J} s_1^- \xrightarrow{D_c} s_1^+ \xrightarrow{R_s^0} s_F \xrightarrow{D_s} I$
$t_2 < t < t_3^J$	$J \xrightarrow{R_s^J} s_{\mathrm{IIb}}^- \xrightarrow{D_c} s_{\mathrm{IIb}}^+ \xrightarrow{D_c} s_\#^{(1)} \xrightarrow{R_s^J} s_1^- \xrightarrow{D_c} s_1^+ \xrightarrow{R_s^0} s_F \xrightarrow{D_s} I$
$t_3^J < t < t_1$	$J \xrightarrow{R_s^0} s_*^{(2)} \xrightarrow{D_c} s_\#^{(2)} \xrightarrow{R_s^J} s_{\mathrm{IIb}}^+ \xrightarrow{D_c} s_{\mathrm{IIb}}^- \xrightarrow{R_s^J} s_\#^{(1)} \xrightarrow{D_c} s_1^- \xrightarrow{D_c} s_1^+ \xrightarrow{R_s^0} s_F \xrightarrow{D_s} I$
$t_1 < t < t_3$	$J \xrightarrow{R_s^0} s_*^{(2)} \xrightarrow{D_c} s_\#^{(2)} \xrightarrow{R_s^J} s_{\mathrm{IIb}}^- \xrightarrow{D_c} s_{\mathrm{IIb}}^+ \xrightarrow{D_c} s_{\mathrm{IIa}}^{(1)-} \xrightarrow{D_c} s_{\mathrm{IIa}}^{(1)+} \xrightarrow{D_s^0} s_1^+ \xrightarrow{R_s^0} s_F \xrightarrow{D_s} I$
$t_3 < t < t_4$	$J \xrightarrow{R_s^0} s_*^{(2)} \xrightarrow{D_c} s_\#^{(2)} \xrightarrow{R_s^J} s_{\mathrm{I2}}^- \xrightarrow{D_c} s_{\mathrm{I2}}^+ \xrightarrow{R_s^0} s_\gamma^- \xrightarrow{D_s} s_\gamma^+ \xrightarrow{R_s^0} s_1^+ \xrightarrow{R_s^0} s_F \xrightarrow{D_s} I$
$t > t_4$	$J \xrightarrow{R_s^0} s_*^{(2)} \xrightarrow{D_c} s_{\mathrm{IIa}}^{(2)-} \xrightarrow{D_c} s_{\mathrm{IIa}}^{(2)+} \xrightarrow{R_s^0} s_\gamma^- \xrightarrow{D_s} s_\gamma^+ \xrightarrow{R_s^0} s_1^+ \xrightarrow{R_s^0} s_F \xrightarrow{D_s} I$

Time step was defined based on CFL criteria:

$$\frac{\Delta t}{\Delta x} \max_p \left|\chi_p\right| \leq \mathrm{CFL},\ p = s, c \tag{62}$$

where $\chi_s = f_s'$ and $\chi_c = \frac{f}{s+a'(c)}$ are the eigenvalues associated to system (9). For all simulations we adopted CFL = 0.99 and $\Delta x = 0.002$. Figures 14, 15, 16, 17 and 18 present saturation and concentration profiles for different simulation times. Note that there is an excellent agreement between the solutions.

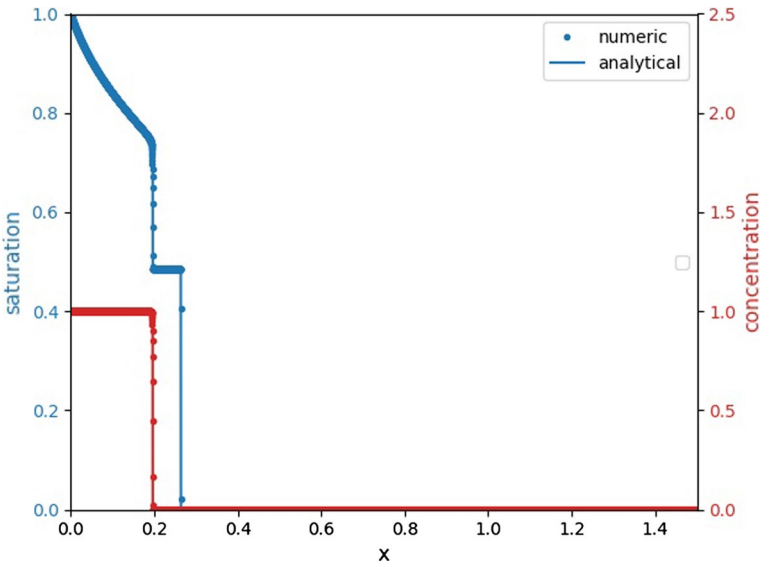

Fig. 14 Analytical and numerical saturation and concentration profiles for $t_D = 0.20$

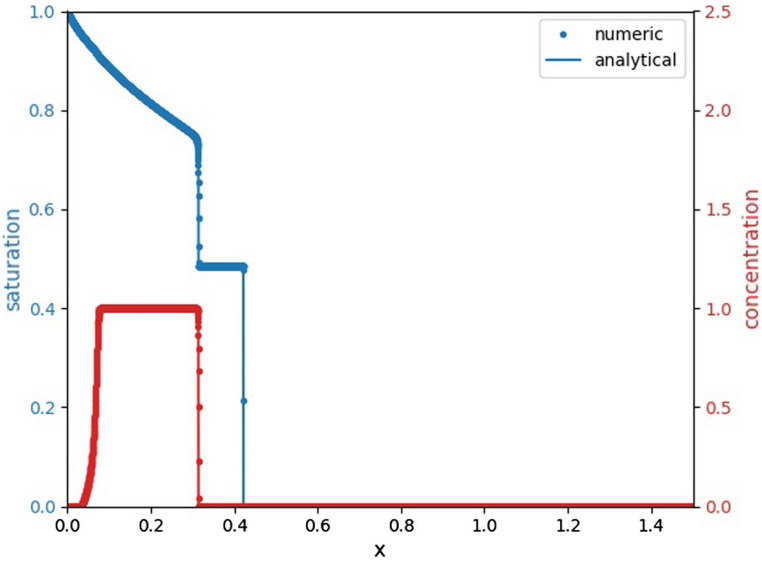

Fig. 15 Analytical and numerical saturation and concentration profiles for $t_D = 0.32$

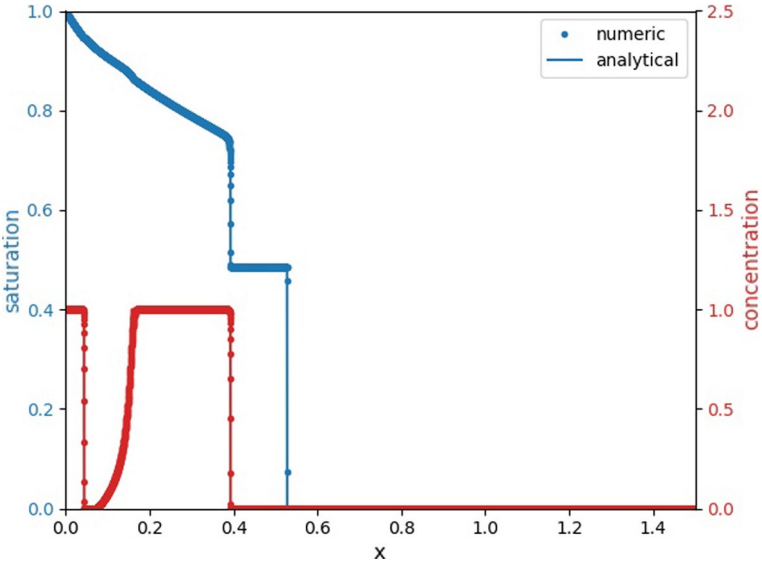

Fig. 16 Analytical and numerical saturation and concentration profiles for $t_D = 0.40$

6 Conclusions

In this paper, we present the analytical solution for the water alternated polymer injection EOR technique. This solution may be applied for any number of polymer slugs with different concentrations, and the polymer may be adsorbed by the rock. The introduction of an auxiliary

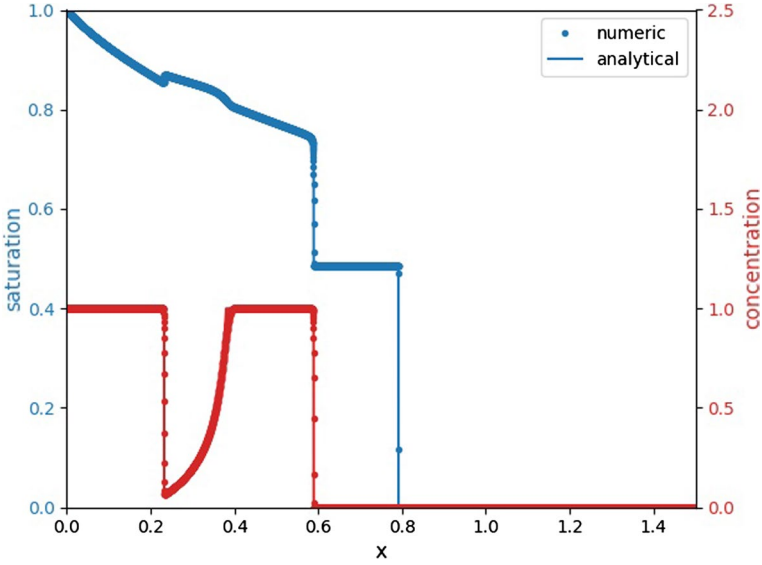

Fig. 17 Analytical and numerical saturation and concentration profiles for $t_D = 0.60$

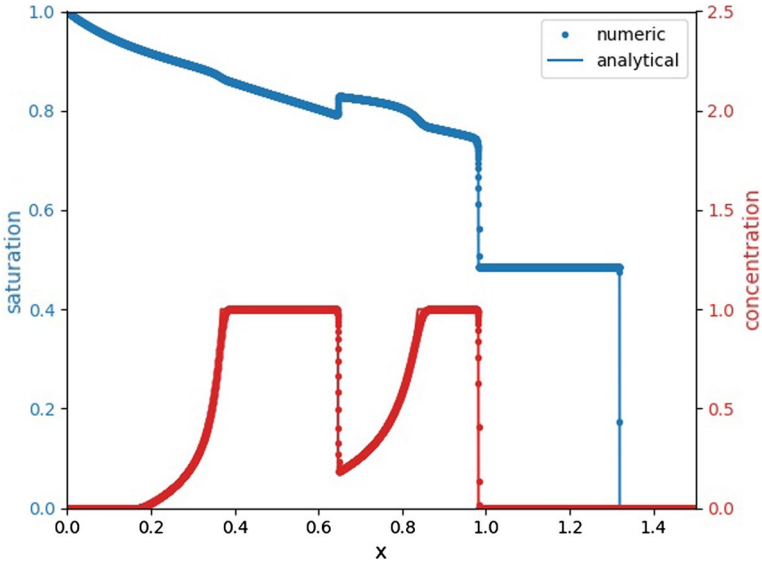

Fig. 18 Analytical and numerical saturation and concentration profiles for $t_D = 1.0$

independent variable splits the conservation system into two independent equations, one based on the thermodynamics features of the problem (adsorption isotherms) and the other dependent on transport properties and the solution of the concentration equation. From the auxiliary equation solution, it is possible to map all the concentration shocks of the original problem. The front slug speed is always greater than the rear speed regardless of the polymer injection

concentration. Therefore, the polymer slugs will catch up with the previously polymer slug injected. The interaction between rarefaction waves of different families is calculated by solving the lifting equation in the regions where concentration changes. This solution is new and has not been investigated. It can also be used as a basis for the evaluation of similar problems (alternated slugs injection). We expect that these results will be relevant to: (i) implementation of the solution in streamline reservoir simulation; (ii) validation of numerical methods; and (iii) the interpretation of polymer flooding experiments.

Appendix

The shock path resulting from the interaction between two simple waves is described in Rhee et al. (1989a) when the rarefaction waves arise from the coordinate axis. Here, the same approach is used to build the trajectory of shocks when the rarefaction waves arise from any curve. Considering that along the path shock x and φ are functions of U^- and U^+, we obtain the following expression to the shock path:

$$\frac{\mathrm{d}\varphi}{\mathrm{d}x} = \frac{F\left(U^+,0\right) - F(U^-,0)}{U^+ - U^-} = \frac{(\partial\varphi/\partial U^-)\left(\mathrm{d}U^-/\mathrm{d}U^+\right) + \left(\partial\varphi/\partial U^+\right)}{(\partial x/\partial U^-)\left(\mathrm{d}U^-/\mathrm{d}U^+\right) + \left(\partial x/\partial U^+\right)} = \tilde{\omega}\left(U^-,U^+\right) \tag{63}$$

Equation (63) can be rewritten as

$$\frac{\mathrm{d}U^-}{\mathrm{d}U^+} = -\frac{\tilde{\omega}\left(\partial x/\partial U^+\right) - \left(\partial\varphi/\partial U^+\right)}{\tilde{\omega}(\partial x/\partial U^-) - (\partial\varphi/\partial U^-)} \tag{64}$$

At an arbitrary point (x, φ) on the shock path we have two characteristics intersecting, one from the curve $\varphi_A(x)$ and another from the curve $\varphi_B(x)$ (Fig. 19). These characteristic curves are straight lines:

$$\varphi = \omega^+\left(x - \xi^+\right) + \eta^+ \quad \text{and} \quad \varphi = \omega^-(x - \xi^-) + \eta^- \tag{65}$$

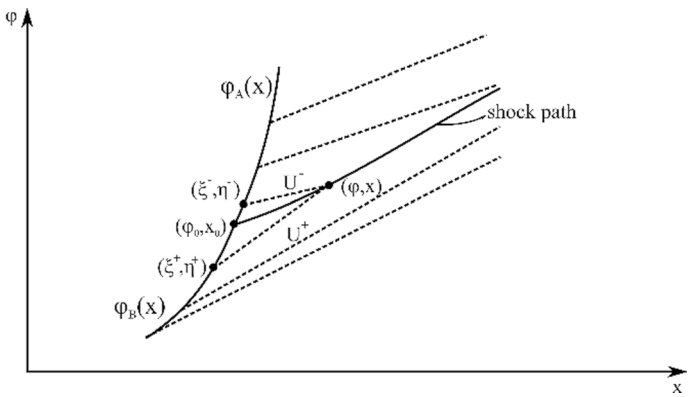

Fig. 19 Shock path arising from the interaction of two rarefaction waves of the same family

where $\omega^{\pm} = F'_U(U^{\pm}, 0)$, $\left(\xi^+ = \xi^+\left(U^+\right), \eta^+ = \eta^+\left(U^+\right)\right)$ and $(\xi^- = \xi^-(U^-), \eta^- = \eta^-(U^-))$ are points on the curves $\varphi_A(x)$ and $\varphi_B(x)$, respectively.

From Eq. (65) we write φ and x as functions of U^- and U^+:

$$x = \frac{\eta^- - \eta^+ + \omega^+\xi^+ - \omega^-\xi^-}{\omega^+ - \omega^-} \quad \text{and} \quad \varphi = \frac{\omega^+\eta^- - \omega^-\eta^+ + \omega^-\omega^+\left(\xi^+ - \xi^-\right)}{\omega^+ - \omega^-} \tag{66}$$

Deriving x and φ with respect to U^+ and U^- and substituting into Eq. (64), we obtain an ordinary differential equation relating U^- and U^+:

$$\frac{\mathrm{d}U^-}{\mathrm{d}U^+} = \frac{\tilde{\omega} - \omega^-}{\tilde{\omega} - \omega^+} \frac{\left(\omega^+ - \omega^-\right)\left(\eta'^+ - \omega^+\xi'^+\right) + \left[\eta^- - \eta^+ + \left(\xi^+ - \xi^-\right)\omega^-\right]\omega'^+}{(\omega^+ - \omega^-)(\eta'^- - \omega^-\xi'^-) + [\eta^- - \eta^+ + (\xi^+ - \xi^-)\omega^+]\omega'^-} \tag{67}$$

where $\omega'^{\pm} = F''_U(U^{\pm}, 0)$, $\eta'^{\pm} = \mathrm{d}\eta^{\pm}/\,\mathrm{d}U^{\pm}$ and $\xi'^{\pm} = d\xi^{\pm}/\,\mathrm{d}U^{\pm}$.

The solution of Eq. (67) allows the determination of U^- for an specified U^+. Replacing U^- and U^+ in Eq. (66), we obtain the shock path.

References

Bedrikovetsky, P.G.: Displacement of oil by a slug of an active additive forced by water through a stratum. Fluid Dyn. **17**(3), 409–417 (1982)

Bedrikovetsky, P.G.: Mathematical Theory of Oil and Gas Recovery. With Applications to Ex-USSR Oil and Gas Fields. Springer Netherlands, Amsterdam (1993)

Borazjani, S., Bedrikovetsky, P., Farajzadeh, R.: Analytical solutions of oil displacement by a polymer slug with varying salinity. J. Petrol. Sci. Eng. **140**, 28–40 (2016a)

Borazjani, S., Roberts, A.J., Bedrikovetsky, P.: Splitting in systems of PDEs for two-phase multicomponent flow in porous media. Appl. Math. Lett. **53**, 25–32 (2016b)

Borazjani, S., Behr, A., Genolet, L., Van Der Net, A., Bedrikovetsky, P.: Effects of fines migration on low-salinity waterflooding: analytical modelling. Transp. Porous Media **116**, 213–249 (2017)

Darcy, H.: Les fontaines publiques de la ville de Dijon. Dalmont, Paris (1856)

Fayers, F.J., Perrine, R.L.: Mathematical description of detergent flooding in oil reservoirs. Paper SPE 1132 presented at the SPE Fall Meeting of the Society of Petroleum Engineers of AIME, Houston, 5–8 Oct (1958)

Hatzignatiou, D.G., Norris, U.L., Stavlandb, A.: Core-scale simulation of polymer flow through porous media. J. Petrol. Sci. Eng. **108**, 137–150 (2013)

Hatzignatiou, D.G., Moradi, H., Stavlandb, A.: Polymer flow through water- and oil-wet porous media. J. Hydrodyn. **27**(5), 748–762 (2015)

Helfferich, F.G.: Theory of multicomponent, multiphase displacement in porous media. SPE J. **21**(1), 51–62 (1981)

Johansen, T., Winther, R.: The solution of Riemann problem for a hyperbolic system of conservation laws modeling polymer flooding. SIAM J. Math. Anal. **19**(3), 541–566 (1988)

Johansen, T., Winther, R.: The Riemann problem for multicomponent polymer flooding. SIAM J. Math. Anal. **20**(04), 908–929 (1989)

Khorsandi, S., Qiao, C., Johns, R.T.: Displacement efficiency for low-salinity polymer flooding including wettability alteration. SPE J. **22**(02), 417–430 (2017)

Lake, L.W., Helfferich, F.: Cation exchange in chemical flooding: part 2—the effect of dispersion, cation exchange, and polymer/surfactant adsorption on chemical flood environment. SPE J. **18**(06), 435–444 (1978)

Leveque, R.J.: Finite Volume Methods for Hyperbolic Problems. Cambridge University Press, Cambridge (2002)

Littmann, W.: Polymer Flooding. Elsevier Science Publishers B.V., New York (1988)

Logan, J.D.: An Introduction to Nonlinear Partial Differential Equations, 2nd edn. Wiley, Hoboken, NJ (2008)

Pires, A.P., Bedrikovetsky, P.G., Shapiro, A.A.: Analytical modeling for two-phase EOR processes: splitting between hydrodynamics and thermodynamics. Paper SPE 89919 presented at the SPE annual technical conference and exhibition, Houston, 26–29 Sept (2004)
Pires, A.P., Bedrikovetsky, P.G.: Analytical modeling of 1d n-component miscible displacement of ideal fluids. Paper SPE 94855 presented at the SPE Latin American and Caribbean petroleum engineering conference, Rio de Janeiro, 20–23 June (2005)
Pires, A.P., Bedrikovetsky, P.G., Shapiro, A.A.: A splitting technique for analytical modelling of two-phase multicomponent flow in porous media. J. Petrol. Sci. Eng. **51**, 54–67 (2005)
Pope, G.A.: The application of fractional flow theory to enhanced oil recovery. SPE J. **20**(3), 191–205 (1980)
Pope, G.A., Lake, L.W., Helfferich, F.G.: Cation exchange in chemical flooding: part 1—basic theory without dispersion. SPE J. **18**(06), 418–434 (1978)
Rhee, H.K., Aris, R., Amundson, N.R.: First-Order Partial Differential Equations, vol. 1. Prentice-Hall, Hoboken, NJ (1989a)
Rhee, H.K., Aris, R., Amundson, N.R.: First-Order Partial Differential Equations, vol. 2. Prentice-Hall, Hoboken, NJ (1989b)
Sekhar, T.R., Sharma, V.D.: Interaction of shallow water waves. Stud. Appl. Math. **121**(01), 1–25 (2008)
Sekhar, T.R., Sharma, V.D.: Wave interactions for the pressure gradient equations. Methods Appl. Anal. **17**(2), 165–178 (2010)
Shen, C.: Wave interactions and stability of the Riemann solutions for the chromatography equations. J. Math. Anal. Appl. **365**, 609–618 (2010)
Smoller, J.: Shock Wave and Reaction–Diffusion Equation, 2nd edn. Springer-Verlag, New York (1994)
Sorbie, K.S.: Polymer-Improved Oil Recovery. Blackie, Florida (1991)
Sun, M.: Interactions of elementary waves for the Aw-Rascle model. SIAM J. Appl. Math. **69**(6), 1542–1558 (2009)
Thiele, M., Batycky, R., Pollitzer, S., Clemens, T.: Polymer-flood modeling using streamlines. SPE Reserv. Eval. Eng. **13**(2), 313–322 (2010)
Torrealba, V.A., Hoteit, H.: Improved polymer flooding injectivity and displacement by considering compositionally-tuned slugs. J. Petrol. Sci. Eng. **178**, 14–26 (2019)
Vicente, B.J., Priimenko, V.I., Pires, A.P.: Semi-analytical solution for a hyperbolic system modeling 1D polymer slug flow in porous media. J. Petrol. Sci. Eng. **115**, 102–109 (2014)
Whitham, G.B.: Linear and Nonlinear Waves. Wiley, New York (1974)
Zarand, M.A.F., Pillai, K.: Spontaneous imbibition of liquid in glass fiber wicks, part II: validation of a diffuse-front model. Transp. Phenomena Fluid Mech. **64**(01), 306–315 (2017)
Zhang, T., Yang, H., He, Y.: Interactions between two rarefaction waves for the pressure-gradient equations in the gas dynamics. Appl. Math. Comput. **199**, 231–241 (2008)
Zhao, S., Pu, W., Wei, B., Xu, X.: A comprehensive investigation of polymer microspheres (PMs) migration in porous media: EOR implication. Fuel **235**, 249–258 (2019)